STRUCTURE-FROM-MOTION BASED VEGETATION MODELING AND SHADE ESTIMATION

A Thesis
by
JAMES NATHANIEL BALCOMB

Submitted to the Graduate School
at Appalachian State University
in partial fulfillment of the requirements for the degree of
MASTER OF ARTS IN GEOGRAPHY

May 2015
Department of Geography and Planning

STRUCTURE-FROM-MOTION BASED VEGETATION MODELING AND SHADE ESTIMATION

A Thesis
by
JAMES NATHANIEL BALCOMB
May 2015

APPROVED BY:

_____
Jeffrey Colby, Ph.D.
Chairperson, Thesis Committee

_____
Chuanhui Gu, Ph.D.
Member, Thesis Committee

_____
Jessica Mitchell, Ph.D.
Member, Thesis Committee

_____
Kathleen Schroeder, Ph.D.
Chairperson, Department of Geography and Planning

_____
Max C. Poole, Ph.D.
Dean, Cratis D. Williams School of Graduate Studies

Abstract

Structure-from-Motion based Vegetation Modeling and Shade Estimation

James Balcomb
B.S., Humboldt State University
M.A., Appalachian State University

Chairperson: Jeffrey D. Colby

Although three-dimensional (3-D) light dimension and range (LiDAR) point cloud datasets describing the structure of vegetation have proven to be highly useful for ecological modeling, the collection of such data is expensive. However, a new technology known as Structure-from-Motion, or SfM, has become available that can be used to create 3-D point cloud datasets for far less cost. A small unmanned aerial system (UAS), point and shoot digital camera, and Agisoft PhotoScan® (*http://agisoft.com*) software were used to create a highly dense 3-D SfM point cloud dataset representing a short reach of the Upper South Fork of the New River in Boone, NC. The quality of the 3-D SfM point cloud dataset was evaluated with an emphasis on how accurately vegetation was represented. Also, a digital surface model (DSM) based on the 3-D SfM point cloud dataset was used in conjunction with a solar ray tracing method to predict shade cast by vegetation in the study area. Overall, the results of this study suggest that SfM based point clouds representing vegetation are of a high enough quality to be used for ecological modeling purposes.

Acknowledgments

I would like to thank my committee members Jeffrey Colby, Jessica Mitchell and Chuanhui Gu for enough advice to keep my thesis within the bounds of scientific standards, but also enough freedom and independence to pursue my own ideas. I would also like to thank Michael Flannigan for his work over the 2013-2014 academic year researching and purchasing the equipment that I used. I greatly benefitted from Michaels wise choices. I would like to thank Jeffrey Colby for pursuing the purchase of said equipment and Kathleen Schroeder for approving the final purchase. I would like to thank Jeffrey Colby and Chuanhui Gu for awarding me GRAM funding, and the Cratis D. William Graduate School for awarding me a Chancellors Fellowship.

Table of Contents

Foreword

The article presented in this thesis will be submitted to *Photogrammetric Engineering & Remote Sensing*, the official journal of the American Society for Photogrammetry and Remote Sensing. The organization and formatting of the article main body strictly follows the instruction to authors for manuscript submission to the journal.

Introduction

In his March 1927 presidential address to the Association of American Geographers (AAG), J. Paul Goode asserted that the map is a "record of progress in geography." Goode argued that maps reflect the current state of geography and that one only need examine a map to understand the abilities and limitations of geographers. Conducting such an examination of contemporary maps would reveal the fact that the field of geography remains limited with regard to its ability to work with three-dimensional (3-D) data. This is not due to the fact that the third, or z coordinate is unimportant but rather that collecting and working with 3-D data has proven to be challenging and expensive. Currently, the most commonly employed method for collecting 3-D data representing the Earth's surface is light detection and ranging (LiDAR). LiDAR represents 3-D geographical data through the use of a 3-D point cloud, which is a dataset composed of anywhere from thousands to millions of individual points representing the location and shape of objects in 3-D space. Each point has an x,y, and z coordinate which places that point in its specific location. Collectively, the points are referred to as a 3-D point cloud dataset. Although highly accurate and proven to produce high quality data, LiDAR is expensive; the use of LiDAR to create 3-D point cloud datasets typically costs tens of thousands of dollars. Such costs make it prohibitive to collect 3-D point cloud datasets at a high temporal resolution, or for small projects or by small organizations. Thus one of the barriers that the field of geography must overcome is finding a method to accurately and inexpensively create 3-D point cloud datasets. Fortunately, technological advances are making possible the production of 3-D point clouds very inexpensively with just a hobbyist grade unmanned aerial system (UAS), a consumer grade digital camera, a desktop computer, and appropriate software packages.

Unmanned Aerial Systems

The first challenge that must be overcome when attempting to collect 3-D point cloud datasets is that of carrying a sensor to an effective height. Traditionally this has been accomplished by the use of a manned aircraft. But it is now possible to use a UAS to easily carry a camera to a height

from which it can take high resolution aerial images. Small UASs can be purchased for less than $2500 and are cheap to operate, making them extremely inexpensive to use.

Consumer Grade Digital Cameras

The second challenge in collecting 3-D geographical data is that of acquiring and operating an appropriate sensor. LiDAR scanners can be expensive and too large to mount on a small UAS. But this issue has been overcome by the fact that for less than $200, a camera can be purchased that weighs less than 300 grams and is able to capture 12 megapixel images. Such a camera can be mounted on a small UAS and capture the images necessary for deriving 3-D geographical data.

Structure From Motion

The third challenge in the process of creating 3-D point cloud datasets is that of measuring the heights of objects using remote sensing techniques. As previously mentioned, LiDAR is expensive, and collecting the images required for traditional photogrammetry requires a high level of expertise and a high level of control over the image capture process. But new techniques in the field of computer vision known as Structure from Motion (SfM) are able to construct 3-D point cloud datasets using a set of overlapping photographs and georeferenced ground control points (GCPs). Such software is ideal for working with images taken using a small UAS.

Justification For The Research Project

While SfM methodologies hold great promise for revolutionizing the field of geography by making possible the inexpensive production of 3-D point cloud datasets, the technology is still new and there is a need to prove the accuracy of the results. Current standards concerning the accuracy of 3-D point cloud datasets have been set by LiDAR collection techniques known as airborne laser scanning (ALS), mobile laser scanning (MBL), and terrestrial laser scanning (TLS). ALS has been found to have a root mean square error (RMSE) ranging from 5.0 cm to 25.9 cm depending on the land cover type while TLS is accepted to have an accuracy rating of a few cm or mm depending on

the circumstances (Hodgson and Bresnahan, 2004). Additionally, United States Geological Survey Quality Level 2 guidelines state that the 95 percent confidence level for a 3-D LiDAR point cloud dataset must be less than or equal to 19.6 cm (Heidemann, 2014). As such, LiDAR collected for use in scientific, commercial, or other professional applications can be expected to adhere to these accuracies.

However, there is not yet a widely accepted accuracy standard for SfM. Nor are the strengths and weaknesses of the technique well understood. Important questions need to be answered such as what is the range of environmental circumstances under which SfM techniques can be used, where do SfM techniques fail to produce accurate results, will SfM capture all objects in a scene equally well, and in general how accurately can SfM data represent features on the Earth's surface?

Problem Statement

In order for SfM to become a useful and widely accepted method of collecting 3-D geographical data, it is necessary to determine the accuracy and reliability of the 3-D point cloud datasets produced. The purpose of this research was to investigate the ability of SfM techniques to represent an area of mixed land cover types including deciduous and coniferous forest, turf grass and a river. Multiple study objectives were as follows:

1. Deploy a UAS system to collect a series of aerial images of a short reach of the South Fork of the New River located in Boone, N.C, USA.
2. Construct a georeferenced 3-D point cloud dataset from the collected images using an SfM process and differential global positioning system (DGPS) unit.
3. Assess the density of the 3-D SfM point cloud dataset to estimate how well different land cover types may be represented.
4. Assess the horizontal and vertical accuracy of the 3-D SfM point cloud dataset by comparing field measurements of tree and building heights with tree and building heights determined using a LiDAR/SfM hybrid DSM.

5. Assess the horizontal and vertical accuracy of the 3-D SfM point cloud dataset by comparing an SfM derived DSM to a LiDAR derived DSM.
6. Assess the horizontal and vertical accuracy of the 3-D SfM point cloud dataset by using an SfM derived DSM in conjunction with the GRASS GIS module r.sunmask (*http://grass.osgeo.org*) to predict patterns of shade cast by objects. (If the three dimensional shape of objects is constructed accurately by the SfM process, then the shade patterns predicted by the GRASS r.sunmask module should match shade patterns in reference photographs.)

Role of the Author

The role of the lead author (James Balcomb) was to serve as the primary investigator for the study and to conduct the following activities:

1. Develop and deploy a UAS system able to collect the photographs necessary for constructing a 3-D SfM point cloud dataset.
2. Collect DGPS data necessary for geo-referencing the aforementioned 3-D point cloud dataset.
3. Construct a 3-D point SfM cloud dataset using the photographs collected in step one and an appropriate software package.
4. Assess the density and horizontal and vertical root mean square error (RMSE) of the 3-D SfM point cloud dataset using ground truthing methods and a 3-D LiDAR point cloud dataset.
5. Predict patterns of shade occurring in the study area using the 3-D SfM point cloud dataset.
6. Conduct an assessment to determine the accuracy with which the shade patterns were predicted.
7. Produce a manuscript documenting the aforementioned steps and results produced.

Structure-from-Motion based Vegetation Modeling and Shade Estimation.

James N. Balcomb, Jeffrey D. Colby, Chuanhui Gu, Jessica Mitchell

Abstract

Although three-dimensional (3-D) light dimension and range LiDAR point cloud datasets representing the structure of vegetation have proven to be highly useful for ecological modeling, the collection of such data is expensive. However, a new technology known as Structure-from-Motion, or SfM, has become available that can be used to create 3-D point cloud datasets for far less cost. A small unmanned aerial system (UAS), point and shoot digital camera, and Agisoft PhotoScan® (*http://agisoft.com*) software were used to create a highly dense 3-D point cloud dataset representing a short reach of the Upper South Fork of the New River in Boone, NC. The quality of the 3-D point cloud dataset was investigated with an emphasis on determining how accurately vegetation was represented. Also, a digital surface model (DSM) based on the 3-D point cloud dataset was used in conjunction with a solar ray tracing method to predict shade cast by vegetation in the study area. Overall, the results suggest that the use of SfM methods to construct 3-D point cloud datasets representing vegetation are of a high enough quality to be used for ecological modeling purposes.

Introduction

Three-dimensional (3-D) light dimension and ranging (LiDAR) point cloud datasets have proven valuable for ecological applications such as modeling riparian shade, determining leaf-area-index (LAI) and estimating above ground biomass (e.g., Greenberg et al. 2012; Lefsky et al. 2002; Newcomb 2012). The use of 3-D LiDAR point cloud datasets in ecological applications is limited by the fact that collecting such data is expensive with even small projects costing tens of thousands of

dollars. Erdody and Moskal (2010) found that collecting LiDAR data cost about US$3.00/Ha plus initial costs ranging from $10,000-20,000, and a study conducted by the United States Forest Service found that it cost $33,424 to collect LiDAR data for 12,792 hectares (Hummel et al., 2011).

However, techniques in computer vision known as Structure-from-Motion, or SfM, combined with advances in unmanned aerial systems (UAS) and digital cameras have created a less expensive alternative for creating 3-D point cloud datasets. The equipment necessary can be purchased for less than $10,000 and includes a hobbyist grade UAS, a consumer grade digital camera, and a software package such as AgiSoft PhotoScan ® (*http://www.agisoft.com*).

Structure from Motion

SfM is a computer vision process able to derive a 3-D point cloud dataset from a set of unordered photographs that may have been taken from a variety of angles and distances (Snavely et al., 2006). The main requirement for generating datasets using SfM is that horizontal image overlap is at least 66% and that vertical image overlap is at least 80%. Strict control over parameters such as focal length, perspective angle, and distance to the target is unnecessary (Snavely et al., 2006). Rather, automated algorithms in the software are able to calculate crucial information such as focal length and the relative position from where an image was taken (Dandois and Ellis, 2013; Snavley et al., 2006).

SfM uses photogrammetric principles and a three step process in the reconstruction of 3-D scene geometry from two dimensional images (Verhoeven, 2011). The first step in the SfM process is to determine internal and external parameters such as camera position and focal length for each photograph in the set (Snavely et al., 2006). This is accomplished through identifying specific features in photographs than can be seen in additional photographs (Snavely et al., 2006). By matching and aligning common features in two photographs it is possible to calculate the relative position of those two photographs to each other. This step is repeated until the relative position of all photographs in the set are identified. Step two utilizes photogrammetric principles and the positional

information of the photographs to construct a sparse 3-D point cloud dataset. Photogrammetry works by using geometrical principles and 2D photographs to determine the location of features in 3-D space (Geodetic Systems, 2014). In order for the image of a feature to be captured in a photograph, lights waves must be reflected from that object through the principle point of the camera lens and onto the cameras sensor surface. Some of these light waves travel in a straight line from the feature to the camera lens, passing directly through the principal point of the camera lens. Since these light waves have traveled in a straight line it is possible to use their location on the cameras sensor, in conjunction with the cameras focal length, to recreate the path that was traveled to reach the sensor. Hence, for a given pixel on the camera sensor it is possible to determine a straight line connecting that specific pixel with the feature from which the light ray originated. By performing this process for multiple, overlapping images, numerous straight lines from unique camera positions to the same feature are created. The point in space where the lines intersect will be the features position in three-dimensional space. Therefore, it can be known relative to the position of the camera what that features x,y, and z coordinates are.

With the positional information of photographs from step one, the previously described photogrammetric principles are used to construct a sparse 3-D point cloud dataset. A sparse point cloud is constructed due to the need to use only matching features that are very clear in the construction of scene geometry (Verhoeven, 2011). Thus the initial 3-D point cloud dataset will necessarily be sparse due to the need to use only the clearest matching features. Step three in the SfM process is the construction of a dense 3-D point cloud by using the reconstructed scene geometry from step two and every single pixel in the photographs to fill in the details between points in the sparse 3-D point cloud dataset (Verhoeven, 2011). Assuming that a pixel is located in an area that overlaps with another photograph, that pixel can be matched with a pixel in the second photograph to create a matching point. With the 3-D geometry of the scene established, the thousands of matching points derived from individual pixels can be used to fill in the areas between points in the sparse 3-D point cloud dataset. The result is the final product, or the dense 3-D point cloud dataset. The

robustness of SfM methods has been demonstrated, for example, by constructing 3-D point cloud datasets of historical sites from internet photo collections where focal length, and camera model were unavailable (Snavley et al., 2006).

Collecting the data necessary to create a 3-D point cloud dataset can be as simple as taking a set of highly overlapping images of an area of interest. However, without any geo-referencing data the 3-D point cloud dataset constructed by the SfM process will be in an arbitrary coordinate system and may not be correctly oriented with regard to the x,y and z axis. Geo-referencing is achieved by establishing the coordinates of specific points located within the 3-D point cloud dataset, and then using a transformation to establish the coordinates of every other point in the dataset. Thus, in order to create a georeferenced 3-D point cloud dataset using the SfM process, both a set of highly overlapping photographs and the x,y, and z coordinates of specific features or ground control points (GCPs) in the photographs are necessary.

Unmanned Aerial Systems

Modern UASs come in a variety of sizes and capabilities, ranging from 1 Kg remote controlled helicopters able to carry only a lightweight camera, to large military style drones capable of carrying advanced weaponry. The UASs of interest for lower budget research projects typically fall into the nano, micro, or mini class (Colomina and Molina, 2014).Such UASs are characterized by light take off weights (less than 15 kg) , short ranges (less than 10 Km), and low operating altitudes (Colomina and Molina, 2014). Additionally, UASs of the nano, micro, or mini class typically have short flight times ranging from ten to forty-five minutes. For example, the senseFly Ebee (senseFly, 2014) micro UAS can fly for 45 minutes and cover 1000 hectares. Although researchers have successfully used other platforms to gather aerial data, including kites and balloons, motorized UASs provide the advantage of being quick to set up and take down, and can fly in a variety of weather conditions and environmental settings (Bryson et al., 2013). Although a manned aircraft able to collect LiDAR data can cover a larger spatial extent, a UAS collecting photographs for SfM can be

flown inexpensively allowing for repeat collections of data and the documentation of ephemeral events such as the annual growth of new leaves in deciduous forests (Dandois and Ellis, 2013).

Digital Cameras

Also necessary for producing inexpensive 3-D point clouds using SfM methods is a lightweight camera. A micro UAS with a payload of only 300 grams is extremely limited in terms of the payload it can carry. But modern consumer digital cameras are lightweight, (often weighing less than 300 grams) and can capture images at up to a 16 megapixel resolution. Additionally, the cost of a quality digital camera is reasonable, with appropriate models available for under $200.

Accuracy of 3-D SfM Point Cloud Datasets

Although SfM methods hold great potential, there is still a need to assess the quality of the 3-D point clouds produced. Results from studies investigating the accuracy of 3-D SfM point cloud datasets are promising and have found them to be comparable to 3-D LiDAR point cloud datasets. Lucieer at al. (2014) used a DEM derived from SfM data to map landslide displacement and found a horizontal RMSE of 7.4 cm and a vertical RMSE of 6.2 cm when 39 individually GPS measured checkpoints (horizontal and vertical accuracies = 2-4 cm) were used as a reference. Harwin et al. (2012) mapped a natural coastal site in Australia and found a vertical accuracy of 2.5 – 4.0 cm when checkpoints established using a TotalStation were compared to the 3-D SfM point cloud dataset. Fonstad et al. (2013) found a vertical RMSE of 1.049 m when an SFM derived DEM was compared to a LiDAR derived DEM.

These studies took place in arid or semi-arid areas with little vegetation and validated the use of SfM for describing earthen features. Less well understood is how accurately SfM can be used for describing vegetative features and there is evidence to suggest that the presence of vegetation negatively impacts the quality of 3-D SfM point cloud datasets. Westoby et al. (2012) compared an SfM derived DEM to a DEM created using terrestrial laser scanning (TLS) and that found that greater deviations between the surfaces existed in areas of dense vegetation than in less vegetated areas.

Fonstad et al (2013) similarly found that differences between an SfM derived DSM and a LiDAR derived DSM were greatest in areas of vegetation.

SfM for Measuring Vegetation

Although the presence of vegetation may decrease the accuracy of a 3-D SfM point cloud dataset, additional studies provide evidence that useful vegetation metrics may still be determined using SfM methods. Dey et al. (2012) found that it was possible to recreate the structure of grapevines using SfM methods. The 3-D point cloud dataset derived was of a high enough accuracy that an appropriate algorithm was able to discern grapes from stems and leaves with a 96% – 98% success rate. Mathews and Jensen (2013) used a 3-D SfM point cloud dataset to estimate leaf area index (LAI) of grape vines. The LAI predicted using the 3-D SfM point cloud dataset was compared to LAI as observed in the field. This analysis was moderately successful with an $r^2 = 0.567$.

More extensive vegetation mapping using SfM has also been successful. Lisein et al. (2013) used a small UAS and SfM methods to develop a forest canopy height model (CHM) for a 200 hectare plot in France. There was a good fit ($r^2 = 0.91$) between individual tree heights as predicted by the SfM CHM and individual tree heights measured in the field. In comparison, the model fit for a LiDAR CHM was $r^2 = 0.94$. Dandois and Ellis (2013) likewise found that SfM can be used to effectively measure forestry metrics such as tree height. In a study conducted in an eastern deciduous forest, an SfM CHM was comparable to a LiDAR CHM for predicting tree heights ($r^2 = .82 – 0.83$ and $r^2 = .83 – 0.84$ respectively). In addition to finding a high level of agreement for individual trees, Dandois and Ellis (2013) found an RMSE of 2.3 m and an r^2 of 0.87 when an SfM DSM and a LiDAR DSM for a forested area were compared.

The purpose of this paper is to investigate the ability of SfM techniques to reconstruct an area of mixed land cover types including deciduous and coniferous riparian forest, turf grass and a river. In particular, the ability of the SfM process to reconstruct complex vegetation will be examined. In so doing the question of how well SfM techniques can be used for the generation of 3-D point cloud

datasets representing vegetation will be addressed. As vegetation represents a significant component of many landscapes, this question must be answered before SfM methods can be used for purposes of ecological modeling. Thus this study will make a contribution to both the field of SfM and the field of ecology by investigating if SfM techniques are able to reconstruct complex vegetation. Multiple study objectives were as follows:

1. Deploy a UAS system to collect a series of aerial images along a short reach of the South Fork of the New River located in Boone, N.C, USA.
2. Construct a georeferenced 3-D point cloud dataset from the collected images using an SfM process and a differential global positioning system (DGPS) unit.
3. Assess the density of the 3-D SfM point cloud dataset to estimate how well different land cover types may be represented.
4. Assess the horizontal and vertical accuracy of the 3-D SfM point cloud dataset by comparing field measurements of tree and building heights with tree and building heights determined using a LiDAR/SfM hybrid DSM.
5. Assess the horizontal and vertical accuracy of the 3-D SfM point cloud dataset by comparing an SfM derived DSM to a LiDAR derived DSM.
6. Assess the horizontal and vertical accuracy of the 3-D SfM point cloud dataset by using an SfM derived DSM in conjunction with the GRASS GIS module r.sunmask (*http://grass.osgeo.org*) to predict patterns of shade cast by objects. (If the three dimensional shape of objects is constructed accurately by the SfM process, then the shade patterns predicted by the GRASS r.sunmask module should match shade patterns in reference photographs.)

Methods

Study Area

The area selected for the study was a 190 meter reach of the South Fork of the New River located in Boone, North Carolina, USA (Figure 1). The study area includes two picnic shelters, a

constructed wetland, an area of closely cropped turf grass, areas of deciduous and evergreen riparian forest, and a reach of the river which was approximately 10 m wide and 60 to 90 cm deep. The area was relatively flat with no features such as hills or steep slopes. The elevation of the site ranges from 942 to 945 m above sea level. Data were collected on August 27, 2014 under leaf-on conditions.

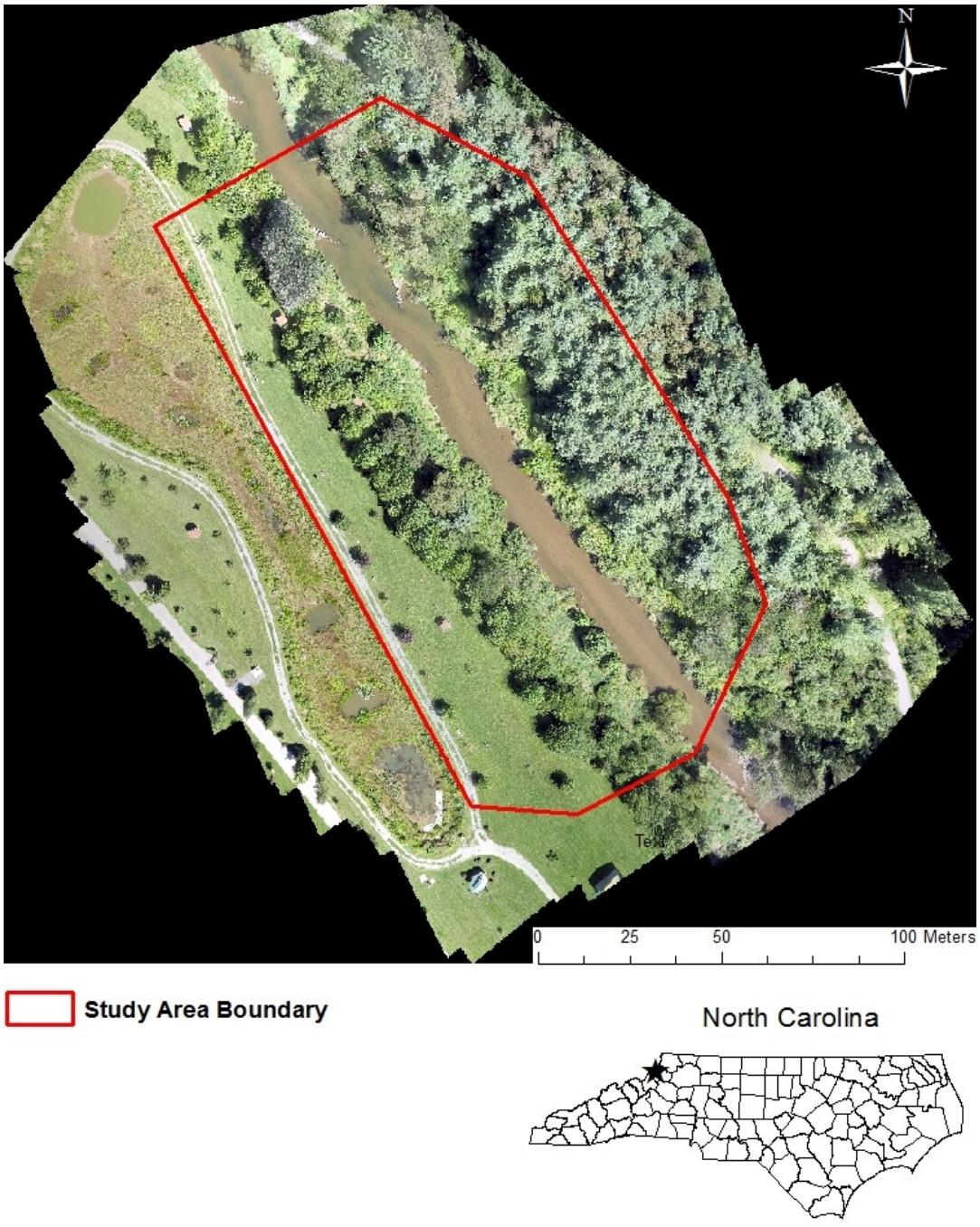

Figure 1. Locator map of the study area.

Data Acquisition

A total of 228 aerial photographs were collected using a Canon PowerShot S100® (Canon U.S.A., 2014) digital point and shoot camera mounted on a DJI Phantom 2 Vision+® quad-copter (DJI, 2014) (Figure 2). A GoPro Hero 4® camera (GoPro, 2014) was also mounted on the quad-copter and used as a means to pilot the aircraft along flight lines (Figure 2). The GoPro camera had a live video feed that was relayed to a small LCD monitor that the operator of the aircraft was able to view (Figure 2). By navigating the quad-copter using the live GoPro video feed it was thus possible to fly a gridded pattern over the study area and capture the necessary aerial photographs for constructing a 3-D SfM point cloud dataset. Flight lines were flown such that photographs had a seventy-five percent horizontal overlap and a ninety percent vertical overlap. Additionally, the DJI Phantom quad-copter had a telemetry data feed that relayed flight parameters, including altitude, to the video monitor. Using this data feed enabled the capture of all photographs from a constant height of approximately seventy meters.

The Canon PowerShot S100 camera was modified to take photographs automatically using the Canon Hack Development Kit (CHDK) (*http://www.chdk.wikia.com*) open source software and additional open source intervalometer script (*http://www.chdk.wikia.com/wiki/countdown_intervalometer*). Through the use of the CHDK/intervalometer software the Canon S100 was programmed to take photographs in a time lapse fashion with one image captured every five seconds (the intervalometer was set to take a photograph every two seconds but post flight analysis found that the interval between image capture was closer to five seconds). Therefore, it was necessary only to initiate the intervalometer function before launching the aircraft and photographs were then captured at a regular interval during flights. The Canon S100 focus was set to infinity and the camera was put in shutter priority mode so that photographs were taken at a shutter speed of 1/1650 seconds.

Figure 2. Equipment used for collecting aerial photographs from left to right: Trimble GeoXH DGPS unit, Go Pro Hero 4 digital camera, Canon S100 digital camera, DJI Phantom Vison 2 +, RX-LCD5802 LCD Monitor, and Futaba flight controller.

Three separate flights were conducted between 11:00 a.m. standard time and 11:45 a.m. standard time on August 27, 2014 with each flight lasting approximately nine minutes. Weather conditions were clear and calm with no clouds present for any of the flights.

A total of nine 46 cm x 46 cm ground control points (GCPs) were distributed throughout the study area prior to image capture. The GPS locations of GCPs were recorded using a Trimble GeoXH® (Trimble Navigation Limited, 2014) differentially corrected DGPS unit (Figure 2). Due to the need to be able to view GCPs in the images, GCP locations were restricted to areas of turf grass and therefore not distributed evenly throughout the study as would be desirable. After the photographs had been captured, five naturally occurring objects (such as boulders in the river and distinct pavement corners) were located in the study area and added as additional GCPs. The addition

of these five objects was made in an attempt to improve the spatial distribution of GCPs in the study area. Thus the total number of GCPs utilized was 14.

The GPS coordinates of the GCPs were corrected using Trimble Correct software run as an ESRI ArcGIS® (*http://www.esri.com*) extension. Elevation values recorded by the GeoXH were in WGS84 height above ellipsoid (HAE) and required further processing in order to be converted to North American Vertical Datum 88 (NAVD88). This conversion was accomplished using VDatum software (*http://vdatum.noaa.gov*) supplied by the National Oceanic and Atmospheric Administration (NOAA). When using the GeoXH to collect data in the field an estimated error bound for each GPS reading is supplied by the GeoXH's software. This information was used to estimate the accuracy of each GCP as ±30 cm (horizontal and vertical).

Data Pre-processing

Construction of 3-D SfM Point Cloud Dataset

The Agisoft PhotoScan Professional software package was used for creating a point cloud from the photographs taken using the Canon S100 and DJI Phantom quad-copter. This process was highly automated with little input required from the user. What user input was required involved geo-referencing and selecting the quality level of the 3-D SfM point cloud dataset.

The first procedure that the PhotoScan software performs is photograph alignment and creation of a sparse 3-D SfM point cloud dataset. Photograph alignment was run with a quality setting of "high" which means that photographs were used at their original resolution as opposed to being coarsened in order to increase processing efficiency (Agisoft, 2014). The Canon S100 camera has a navigation grade GPS and tags every photograph with latitude, longitude and elevation coordinates (WGS84). These values are used by the PhotoScan software to roughly match up the photographs and improve the processing time but they are not accurate enough to geo-reference the final 3-D point cloud dataset. Consequently, the initial sparse point cloud was roughly geo-referenced to WGS84 coordinates but further refined in order to increase the geolocation accuracy level.

In order to improve the geo-referencing of the sparse 3-D SfM point cloud dataset it was necessary to use the GCPs established during the data capture process. First GCP locations were established in all photographs by using the PhotoScan software to locate the center of each target. Once the location of a GCP had been established the corrected GPS coordinates of that target were entered into PhotoScan. When all the GCPs had been located in the photographs and corresponding GPS coordinates entered, an optimization step was run that utilized the location of the GCPs to improve photograph alignment and geo-referencing. The result of the optimization step was a sparse 3-D SfM point cloud dataset georeferenced (WGS84 and NAVD88) using data collected with the GeoXH GPS unit.

The second procedure that PhotoScan software performs is to create a georeferenced 3-D SfM dense point cloud dataset using the georeferenced 3-D sparse point cloud dataset. When referring to the 3-D SfM point cloud dataset, "sparse" and "dense" are relative terms and used to establish the fact that the initial 3-D SfM point cloud dataset contains a lower density of points than the final 3-D SfM point cloud dataset. In this study, the initial "sparse" 3-D SfM point cloud dataset had a density of 15 points/m^2 and the final "dense" 3-D SfM point cloud dataset had a density of 1193 points/m^2. When initiating the creation of the dense 3-D SfM point cloud dataset the PhotoScan software gives the user a choice between "aggressive" or "mild" filtering parameters. Initial trial runs revealed that setting the depth filtering parameter to "aggressive" resulted in the exclusion of some darkly colored trees in the study area. Additionally, the PhotoScan manual (Agisoft, 2014) suggested setting the depth filtering parameter to "mild" in order to aid in the reconstruction of complex objects. Based on both initial observations and the PhotoScan manual the depth filtering parameter was set to "mild". With the quality level set to 'high" and a computer with two Intel(R) Xeon(R) 3.16 Ghz processors, 32.0 GB RAM and a 64-bit operating system used for processing, the processing time required to produce the 3-D SfM dense point cloud dataset was approximately fifty-three hours. A quality level of "high" means that four different processes were run to create the dense 3-D SfM point cloud resulting in points that were more accurate in terms of their location and RGB value (Verhoeven,

2011). Upon completion, the 3-D SfM dense point cloud dataset was converted from WGS84/NAVD88 to North Carolina State Plane coordinate system (NAD83) and exported as an LAS file. The conversion to the North Carolina State Plane system was done in order to match the coordinate system of the 3-D LiDAR point cloud dataset used for comparison purposes.

Editing of the Dense 3-D SfM Point Cloud Dataset

In order to identify and remove any points representing noise, the dense 3-D SfM point cloud dataset was edited using TerraScan® (*http://www.terrasolid.com*) software. The dense 3-D SfM point cloud dataset that was produced by the PhotoScan software had a number of points that were below the surface of the ground. This offset was made apparent by viewing the dense 3-D SfM point cloud dataset from a number of angles using the TerraScan software. (Setting the depth filtering parameter in PhotoScan to "mild" resulted in more subsurface noise points and hence required a greater amount of editing in TerraScan.) Points below an elevation value of 940 m above sea level were clearly below any landscape feature in the study area and were classified as noise and deleted from the point cloud. Isolated points existing greater than two meters from any other point were similarly deleted from the point cloud. Individual points clearly below any landscape feature that had not been deleted by the height filtering method were manually identified using cross section views and deleted. As an additional editing step the dense 3-D SfM point cloud dataset was cropped to only include areas that had been captured from all directions (north, east, west and south) in the photographs. Photographs were manually inspected in order to determine areas not captured from all directions. As a result the dense 3-D SfM point cloud dataset was cropped to include only areas meeting this multi-direction criterion.

3-D LiDAR Point Cloud Dataset

The 3-D LiDAR point cloud dataset used for this study was collected in April, 2010 by Tuck Mapping Solutions of Big Stone Gap, Virgina. The vertical RMSE of the 3-D LiDAR point cloud dataset was 5 cm and the horizontal RMSE was 38 cm. The LiDAR sensor make and model was a

Riegl Q680i with a scan angle of 60 degrees. The 3-D LiDAR point cloud dataset was collected using a helicopter flying at an altitude of 700 meters and a speed of 70 knots. Tuck Mapping Solutions delivered both an all return LiDAR point cloud dataset containing earth, vegetation, and buildings and a bare earth LiDAR point cloud dataset. TerraScan software was used by the authors to further process the all return LiDAR point cloud dataset into a first return LiDAR point cloud dataset. SfM techniques cannot penetrate vegetation and therefore result in a 3-D point cloud dataset similar to a LiDAR first return point cloud. Using a first return 3-D LiDAR point cloud dataset allowed for valid comparisons to be made with the 3-D SfM point cloud dataset. Table 1 illustrates the fact that both the bare earth and the first return 3-D LiDAR datasets were highly dense and also provides density values for the 3-D SfM point cloud as a comparison.

Table 1. LiDAR and SfM 3-D Point Cloud Dataset Characteristics

3-D Point Cloud Dataset	Average Point Density (m^2)	Average Point Spacing (cm)
LiDAR Bare Earth	3.6	40.5
LiDAR First Return	9.8	40.5
SfM	1193	3.9

Geo-referencing Correction

The geo-referencing error of the dense 3-D SfM point cloud dataset was estimated using the first return 3-D LiDAR point cloud dataset as a reference. The first return 3-D LiDAR point cloud dataset was chosen to be used as a reference as it was professionally produced and had a known level of geo-referencing error. This step was completed by using TerraScan software to determine the difference in location between picnic shelters in the LiDAR point cloud and picnic shelters in the SfM point cloud. The *x*, *y* and *z* coordinates of picnic shelter corners were first determined in the LiDAR point cloud and then also determined in the SfM point cloud. This resulted in eight points of comparison (four corners each for two picnic shelters). Based on the differences in coordinates between corresponding corners of picnic shelters in the LiDAR point cloud and the SfM point cloud, an estimate of the geo-referencing error of the SfM point cloud was made. It should be noted that this method of estimating geo-referencing error is not as robust as one with multiple reference locations

spread throughout the study area; however, due to limitations with this particular study it was the method available and provided a useful estimate of geo-referencing accuracy.

The average difference between the locations of picnic shelter corners in the 3-D SfM point cloud dataset and the 3-D Lidar point cloud dataset was found to be 26 cm horizontal and 2 cm in the *z* dimension. The 3-D SfM point cloud dataset appeared to be shifted slightly to the southeast with respect to the 3-D LiDAR point cloud dataset. The geo-referencing accuracy of the 3-D SfM point cloud dataset as determined from using the LiDAR point cloud and picnic shelters was within what would be considered reasonable given that the GeoXH is not considered a survey grade GPS receiver.

Based on the geo-referencing error that was found in the previous step, a final pre-processing step was added whereby the dense 3-D SfM point cloud dataset was transformed slightly in order to minimize the geo-referencing error between the dense 3-D SfM point cloud dataset and the LiDAR 3-D point cloud dataset. Sixteen cm was subtracted from the *x* coordinates and 21 cm was added to the *y* coordinates for all points in the dense 3-D SfM point cloud dataset. The *z* SfM coordinates were left unaltered due to the fact that differences between the SfM and the LiDAR 3-D point cloud datasets in the *z* dimension were minimal.

Construction of Digital Elevation and Digital Height Models

In total, three 2.5-D digital surface feature elevation raster layers were created using the dense 3-D SfM point cloud dataset and the 3-D LiDAR point cloud datasets. The first 2.5-D DSM used only the dense 3-D SfM point cloud dataset. This product is hereafter referred to as the SfM DSM. Cell values in the SfM DSM were determined using the maximum elevation of any SfM point found in a cell area. Areas lacking SfM points were interpolated using a natural neighbor algorithm. To determine the resolutions of the DSM, the following equation was used (Tobler 1988, Turner et al., 2013):

$$d = \sqrt{(A/n)} \quad (1)$$

(where d = average horizontal resolution, A = map area in square meters, and n equals the number of points). It was determined that a resolution as high as 2.9 cm was possible for the SfM DSM. However, when the SfM DSM was used for the additional step of shade modeling, a resolution of 2.9 cm resulted in processing times of several hours. In the interest of efficiency, a coarser cell size of 15 cm was used as the final resolution of the SfM DSM which allowed for the shade modeling process to be run in less than one hour.

The second 2.5-D surface model produced is referred to as the LiDAR/SfM-canopy height model (LIDAR/SfM CHM) and displayed heights of trees and the picnic shelters above ground level. As all cell values in the SfM DSM were in meters above sea level, the heights of individual objects were also in meters above sea level and it was impossible to determine how tall trees and buildings were. In order to overcome this limitation, a CHM was created to calculate the heights of objects above the ground rather than in height above sea level. To accomplish this, first a DEM was created from the bare earth 3-D LiDAR dataset. Based on the average spacing of the bare earth 3-D LiDAR dataset (40.5 cm), the resolution of the bare earth DEM was set to 150 cm. An SfM DSM with a matching resolution of 150 cm was also created using the 3-D SfM point cloud dataset. A resolution of 150 cm was chosen in order to facilitate picking out the tops of trees in the SfM/LiDAR DSM. Cell values in the SfM DSM were determined using the maximum elevation of any SfM point found in a cell area. Subtracting the LiDAR derived bare earth DEM from the SfM DSM resulted in the creation of SfM/LiDAR CHM.

A third DSM was created to display differences between the SfM DSM derived from the dense 3-D SfM point cloud dataset and the first return LiDAR point cloud dataset. This DSM is referred to as the DSM-Diff and was created by subtracting a DSM based on the first return LiDAR point cloud dataset from the SfM DSM. An issue obfuscating the comparison between the dense 3-D SfM point cloud dataset and the first return LiDAR point cloud dataset was the fact that slight differences in the boundaries of the point cloud datasets resulted in DSMs with slightly different

boundaries and cells that did not line up perfectly. To overcome this problem, the extent of the dense 3-D SfM point cloud dataset was edited to match the extent of the first return LiDAR point cloud dataset. This was achieved by thinning the dense 3-D SfM point cloud dataset to include only points existing within 3 horizontal centimeters of a LiDAR point. A Python script was created that thinned the dense 3-D SfM point cloud dataset by matching the x and y coordinates of LiDAR points with the x and y coordinates of SfM points. In order to be considered a match an SfM point had to fall within 3 horizontal centimeters of a LiDAR point. Any non-matching SfM points were deleted. By matching SfM points to LiDAR points the boundaries of the point clouds were almost exactly the same and the resulting DSMs aligned perfectly. In addition, with these comparably dense data sets, representing the DSMs at the same resolution is possible and straightforward to calculate.

Based on the average spacing of the first return LiDAR point cloud (42.6 cm) and thinned 3-D SfM point cloud dataset (42.6 cm), the resolution of both DSMs were set to 90 cm. A resolution of 90 cm was chosen in order minimize interpolation when creating the DSMs. By roughly doubling the average spacing of the both 3-D point cloud data sets, each cell of the DSMs contained on average two points. The max value of any point falling within a cell area was used to determine the value of that cell. The final step in creating the DSM-Diff was to subtract the LiDAR DSM from the DSM based on the thinned 3-D SfM point cloud dataset.

Diagnostic Methods

Measurement of 3-D SfM Point Cloud Dataset Densities

Three dimensional SfM point cloud dataset densities were calculated by randomly selecting thirty points located within each of the four land cover types (flat turf, deciduous forest, river, and conifer forest) and using a tool for calculating point density in TerraScan to determine the density at each point location. The size of the tools bounding box was set to one square meter. By locating the center of the bounding box over the randomly selected points, the SfM point cloud density at that location was reported by the TerraScan software.

Relative Vertical Error of Turf Areas

Thirty randomly selected plots with a radius of 90 cm were selected within flat turf areas. A radius of 90 cm was selected as it was the minimum plot size encompassed more than 30 LiDAR points and more than 30 SfM points allowing for valid statistics to be calculated. The mean and standard deviation of z values for SfM points located within each plot were calculated. Additionally, the RMSE of each plot was determined using the DSM-Diff. For this step the center point of each plot was located on the DSM-Diff and the corresponding cell value noted. These values were used as the basis of the RMSE for flat turf areas.

Measurement of Picnic Shelters and Tree Heights

The vertical and horizontal accuracies of the SFM point cloud were investigated by comparing field measured heights of objects in the study area against SfM measured heights of objects in the study area. Two picnic shelters in the study area were used for this purpose. As each of these structures were less than 270 cm high measuring their dimensions was straightforward and a measuring tape was used to find the distance from the ground to each corner and two roof peaks. In addition, the length of each side of the roof of the picnic shelters was also measured. For each picnic shelter this resulted in a total of six height and four horizontal measurements of centimeter level accuracy.

SfM picnic shelter heights were determined from the SfM DSM using ArcMap software. As each picnic shelter was surrounded by open turf area it was possible to measure their height in the SfM DSM without using the LiDAR bare earth layer as a reference.

Horizontal picnic shelter dimensions were determined from the dense 3-D SfM point cloud dataset using TerraScan software. This method was chosen in order to minimize inaccuracies associated with measuring horizontal distances in a raster layer. As the cell size in the SfM DSM was 15 cm, the resolution was too coarse to measure picnic shelter roof lengths with centimeter accuracy.

However, working with the dense 3-D SfM point cloud dataset directly in TerraScan allowed for measuring picnic shelter roof lengths with a centimeter level of accuracy.

In addition to picnic shelters, the heights of forty-one trees in the study were also measured using an inclinometer and measuring tape. Rather than selecting trees in a randomized fashion, only trees where the crown was clearly visible and the distance to the base could be accurately measured were used. This approach was chosen as it aided in ensuring that the measurement of tree heights was as accurate as possible. Location of individual trees was recorded using a GeoXH DGPS unit. In areas of dense forest GPS readings were taken at three locations in a triangular fashion around the base of the tree. This technique ensured that the correct tree could be picked out in the SfM/LiDAR CHM.

Unlike the picnic shelters, most trees were surrounded by vegetation and it was not possible to determine their height from the SfM DSM. To overcome this problem the LiDAR/SfM CHM was used as the basis for determining SfM tree heights. First, measured tree locations were mapped on the LiDAR/SfM CHM using the recorded GPS data. As these points recorded the base of the tree, they were not an exact match with the highest point of the tree. The highest point of the tree was therefore determined by using the greatest cell value found closest to the GPS recorded tree base. In the deciduous forest area trees were spaced out and it was obvious which tree top matched a GPS recorded tree base. In the evergreen forest trees were dense and it was more challenging to pick out the correct tree top. However, the multiple GPS recordings taken for each evergreen tree made it possible to match field measured trees with trees in the LiDAR/SfM CHM layer.

Shade Modeling

As a further step to investigate the accuracy of the SfM point cloud, the SfM DSM was used as a basis for predicting shade patterns cast by objects in the study area. Although measuring the heights of trees can validate that the highest points of objects are being accurately represented by the SfM process, the question still needs to be answered as to whether or not other aspects of objects, such as width and shape, are also being accurately reconstructed. Shade modeling can assist with this

question by providing insight into the 3-D shape of objects as captured by the dense 3-D SfM point cloud dataset. The logic underlying this process is that shade patterns directly reflect the shape of the objects casting the shade. Thus it is possible to infer from the shape of a shade pattern the 3-D shape of the associated object. As such, if shade patterns are accurately predicted using the SfM DSM then evidence is provided for the fact that the dense 3-D SfM point cloud has accurately reconstructed the shapes of objects found in the study area.

In order to model shade patterns using the 2.5-D SfM DSM the GRASS GIS r.sunmask (*http://grass.osgeo.org*) module was used. This application employs the National Renewable Energy Labs (NREL) SOLPOS algorithm (*http://rredc.nrel.gov/solar/codesandalgorithms/solpos)* in conjunction with a ray tracing model and a DSM to determine areas receiving either shade or sun for a specific date and time. The output is a binary raster file with values of either sun or shade. This application was selected as its accuracy is supported by Ruiz-Arias et al. (2009), who found strong agreement between measured irradiation values and GRASS GIS r.sunmask predicted irradiation values under clear sky conditions ($r^2 = 0.92 – 0.93$). Additionally, Greenberg et al. (2012) found an overall accuracy of 92% when the GRASS GIS r.sunmask module and a LiDAR DSM were used to predict areas of shade in the San Joaquin River Delta. The high resolution 15 cm SfM DSM was used as input for the GRASS GIS r.sunmask module and the time and date set to match that of the original data collection time and date of August 27, 2014 11:30 am Eastern Standard Time. The GRASS GIS r.sunmask module assumes clear sky conditions when predicting shade which matched the clear sky conditions present during the data collection process.

The accuracy of the shade patterns produced was assessed using two different approaches. The first method was an accuracy assessment that evaluated the SfM shade map against shaded areas represented on a reference ortho-image using 200 stratified random points in the study area. One hundred random points were selected from areas predicted to be shaded and one hundred random points were selected from areas predicted to be non-shaded. This distribution pattern ensured that the

results were not biased by the fact that a greater area of the study area was not shaded for the time being modeled.

The reference ortho-image was produced using the PhotoScan software and was constructed from the same images that were used to create the dense 3-D SfM point cloud dataset. In addition, these images made an excellent reference from which to validate shade patterns as they were taken from a low altitude, and the shade patterns cast by trees and other objects were clearly visible.

All 200 points were evaluated using ArcMap software. First, a reference binary raster layer of shade was created by using the ArcMap Raster Algebra Tool to extract all cells with a brightness value of less than fifty from the ortho-image. The brightness value of fifty was determined by using a heuristic approach combined with visual inspections to create a reference raster shade layer matching shaded areas in the reference ortho-image. The ArcMap Resample tool was then used to set the resolution of the reference binary shade layer to 15 cm to match the resolution of the SfM shade map. A reference point was classified as shaded if it fell within a shaded pixel on the reference raster layer. Similarly, a reference point was classified as non-shaded if it fell outside of a shade pixel on the reference layer. With all 200 reference points classified as shade or non-shade the accuracy assessment was completed by comparing the value of reference points to the value of the sample points in the SfM shade map. In addition, shade accuracy was also assessed at 138 stratified random points located only in flat areas such as ground or river, rather than anywhere in the study area. Seventy-nine points were selected from flat shaded areas and seventy-nine points from flat non-shaded areas. A reference point was classified as shaded if it fell within a shaded pixel on the reference raster layer. Similarly, a reference point was classified as non-shaded if it fell outside of a shade pixel on the reference layer. With all 138 reference points from flat areas classified as shade or non-shade the accuracy assessment was completed by comparing the value of reference points to the value of the sample points in the SfM shade map.

The second assessment method compared SfM shade map patterns to reference shade patterns for selected individual trees and one picnic shelter. Only isolated trees located in open turf areas

where shade patterns could clearly be identified were used in this step. First, the binary raster shade reference layer created for the previous accuracy assessment method was used to create polygons of shade shapes for individual trees using the ArcMap "Raster to Polygon" tool. Similarly, the SfM shade map was used to create polygons of shade shapes for the same individual trees. Symmetry between reference shade polygons and SfM shade map polygons was assessed by comparing the symmetric difference of their areas and shapes using the following equation (Colby and Dobson, 2010; Guedot et al., 2004):

$$\text{Error}(\%) = \left(\frac{\text{Area}(\text{Poly}) + \text{Area}(\text{RefPoly}) - 2x\text{Area}(\text{Poly} \cap \text{RefPoly})}{\text{Area}(\text{RefPoly})}\right) x\ 100 \qquad (2)$$

where Poly is the polygon of the predicted shade shape and RefPoly is the polygon of the ortho-image shade shape.

Results

3-D SfM Point Cloud Dataset Characteristics

The final 3-D SFM point cloud covered an area of approximately 17,500 m^2 and contained 20,884,427 points with an average spacing of 3.9 cm and an average density of 1193 points/m^2. All four land cover types were well represented although their point densities varied (Table 2). Flat turf areas had an average point density of 604 points/m^2 and contained little noise as evidenced by a low standard deviation among z values. The average standard deviation among points for thirty samples of turf was 2.0 cm. The river bed had a similar point density with an average of 644 points per m^2 and likewise contained little noise as evidenced by a standard deviation of 1.7 cm amongst points for thirty sample areas. Areas of evergreen and deciduous forest also appeared well constructed with average point densities of 1954 points/m^2 and 1480 points/m^2 respectively. Although the deciduous and conifer forests had greater point densities, points were less evenly distributed than in turf areas or

the river. Some areas of deep shadow were completely lacking in points which left several gaps in both the deciduous and conifer forest point clouds. For thirty sample areas in the deciduous forest, densities ranged from 635 points/m^2 to 2744 points/m^2. For thirty samples in the evergreen forest, densities ranged from 140 points/m^2 to 4284 points/m^2. In contrast, densities for thirty turf samples ranged from 566 points/m^2 to 759 points/m^2 and densities for thirty river samples ranged from 579 points/m^2 to 624 points/m^2.

Table 2. 3-D SfM Point Cloud Densities by Land Cover Type.

Area	Average Density (m^2)	Max Density (m^2)	Min Density (m^2)	Range
Turf	604	759	566	193
River	644	624	579	45
Deciduous forest	1480	2744	635	2109
Conifer forest	1954	4284	140	4144

The very high density of the point cloud, in combination with RGB values determined from the images, created a final product that had a photographic like appearance (Figure 3). As such, the point cloud had a high level of detail and features such as medium sized rocks and sediment lines in the river were discernible. In Figure 3 the features that can be discerned, such as trees and shrubs are formed by the SfM points and the black areas are locations where there is no data due to a lack of points. Figure 3 illustrates various views of strictly the 3-D SfM point cloud dataset. In effect, a three dimensional photo was created with which a viewer could gather useful information such as the type of land cover, river morphology and the relative heights of vegetation.

Figure 3. Nadir (A and B) and oblique (C and D) view of the dense 3-D SfM point cloud dataset. Points are displayed by RGB value.

RMSE of Vegetation And Buildings

The model fit between field measured tree heights and tree heights from the SfM point cloud was very good with r^2 = .96 and an RMSE = 1.25 m (Figure 4). There was a slight tendency for SfM measured tree heights to be lower than field measured tree heights with 61% of SfM measured tree heights lower than corresponding field measured tree heights. This is likely due to the fact that SfM processes can have difficulty with identifying tall thin objects such as the highest branch forming the peak of a tree crown (Liesein et al., 2013). The result of missing the tallest branch would be a slightly

shorter tree in the 3-D SfM point cloud dataset. In contrast, the technique employed to field measure trees reliably picked out tall individual branches forming the highest point of a tree crown.

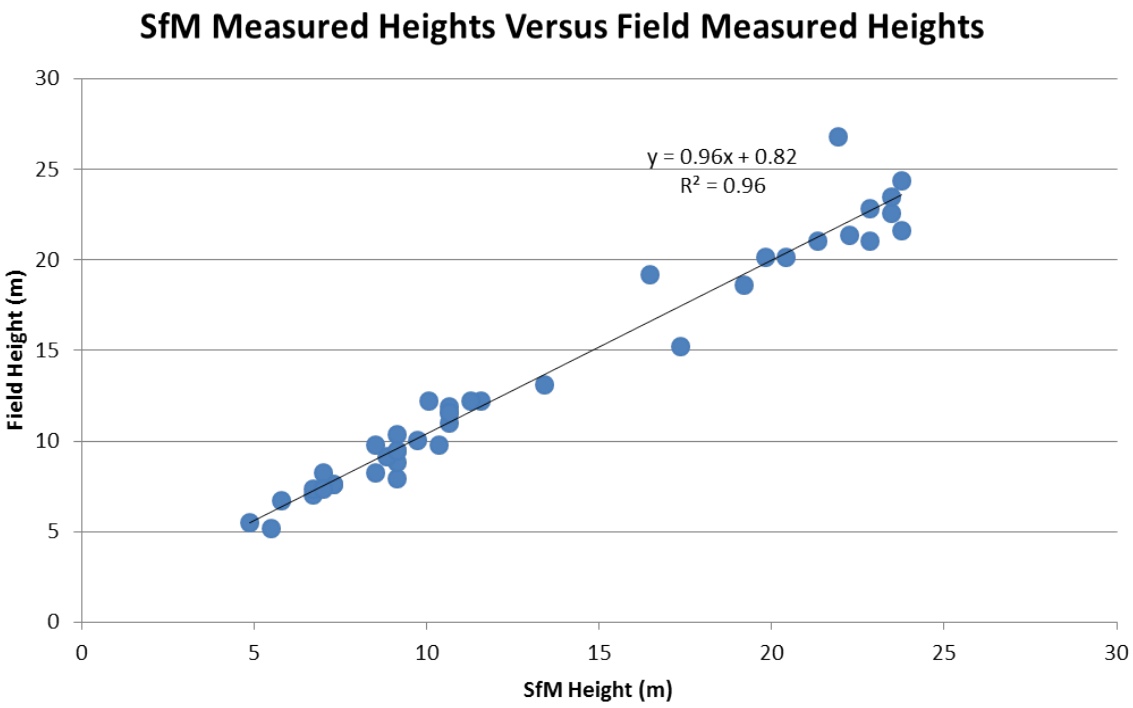

Figure 4. SfM measured tree and building heights versus field measured tree and building heights.

The fit between ground measured picnic shelter heights and SfM DSM picnic shelter heights was also good with a vertical RMSE = 9.6 cm. As a reference, the vertical RMSE between field measured picnic shelter heights and picnic shelter heights from the LiDAR-DSM was 7.1 cm. However, both picnic shelters were not represented by the SfM DSM with the same degree of accuracy. As can be seen in Table 3 there was consistently a higher level of height error associated with the north shelter than with the south shelter. The southern picnic shelter was represented more accurately as evidenced by a vertical RMSE = 8.85 cm. This is in contrast with the poorer results from the northern picnic shelter which had a vertical RMSE = 12.65 cm.

Table 3. SfM DSM Measured Picnic Shelter Heights versus Ground Measured Picnic Shelter Heights

	Field Height	SfM Height North Shelter	SfM North Shelter Error	SfM Height South Shelter	SfM South Shelter Error
Corner 1	240	235	5	236	4
Peak 1	280	260	20	274	6
Corner 2	240	248	-8	246	-6
Corner 3	240	228	12	247	-7
Peak 2	280	266	14	276	4
Corner 4	240	229	11	240	0

Horizontal dimensions of picnic shelters as determined directly from the dense 3-D SfM point cloud dataset were approximately 3% larger than horizontal dimensions as measured in the field. Table 4 displays the differences between ground measured horizontal picnic shelter dimensions and 3-D SfM point cloud dataset measured horizontal picnic shelter dimensions. Both picnic shelters were square with each side of a roof measuring 244 cm. The average length of picnic shelter sides as determined from the SfM point cloud was 252 cm. The average length of a side for the southern shelter was more accurate than for the northern shelter, with average lengths of 248 cm and 256 cm respectively. The horizontal RMSE between field measured picnic shelter lengths and SfM measured picnic shelter lengths was 9.0 cm. Once again, the southern picnic shelter was represented more accurately with a horizontal RMSE = 4.5 cm while the northern picnic shelter had a horizontal RMSE = 12 cm.

Table 4. 3-D SfM Point Cloud Measured Picnic Shelter Horizontal Dimensions versus Field Measured Picnic Shelter Horizontal Dimensions

	Field Length (cm)	SfM North Shelter (cm)	SfM North Shelter Error (cm)	SfM South Shelter (cm)	Sfm South Shelter Error (cm)
North Side	244	255	11	250	6
East Side	244	254	10	245	1
South Side	244	259	15	246	2
West Side	244	255	11	250	6
Average	244	256	11.75	248	3.75

The SfM DSM and the LiDAR DSM were moderately well matched with an overall RMSE = 2.7 m (Table 5). Also seen in Table 5 is that the fit for areas of flat turf was better than for either areas of deciduous or conifer forest.

Table 5. Root Mean Square Error Between 3-D SfM Point Cloud Dataset and 3-D LiDAR Point Cloud Dataset by Land Cover Type

Area	RMSE (m)
Overall	2.7
Turf	0.0094
Deciduous forest	3.7
Conifer forest	3.2

Figure 5 presents an overview of the DSM-Diff. As can be seen in this figure, for the majority of the study area SfM DSM elevation values were greater than LiDAR DSM elevation values. This is an interesting result given that theoretically the difference between the SfM DSM and LiDAR DSM should be minimal and the image seen in Figure 5 should be an even light blue layer. But the differences between the SfM DSM and the LiDAR DSM are such that almost all features in the study area can be discerned. This suggests that the heights for all features as determined from the 3-D SfM point cloud dataset were different than heights as determined from the 3-D LiDAR point cloud dataset.

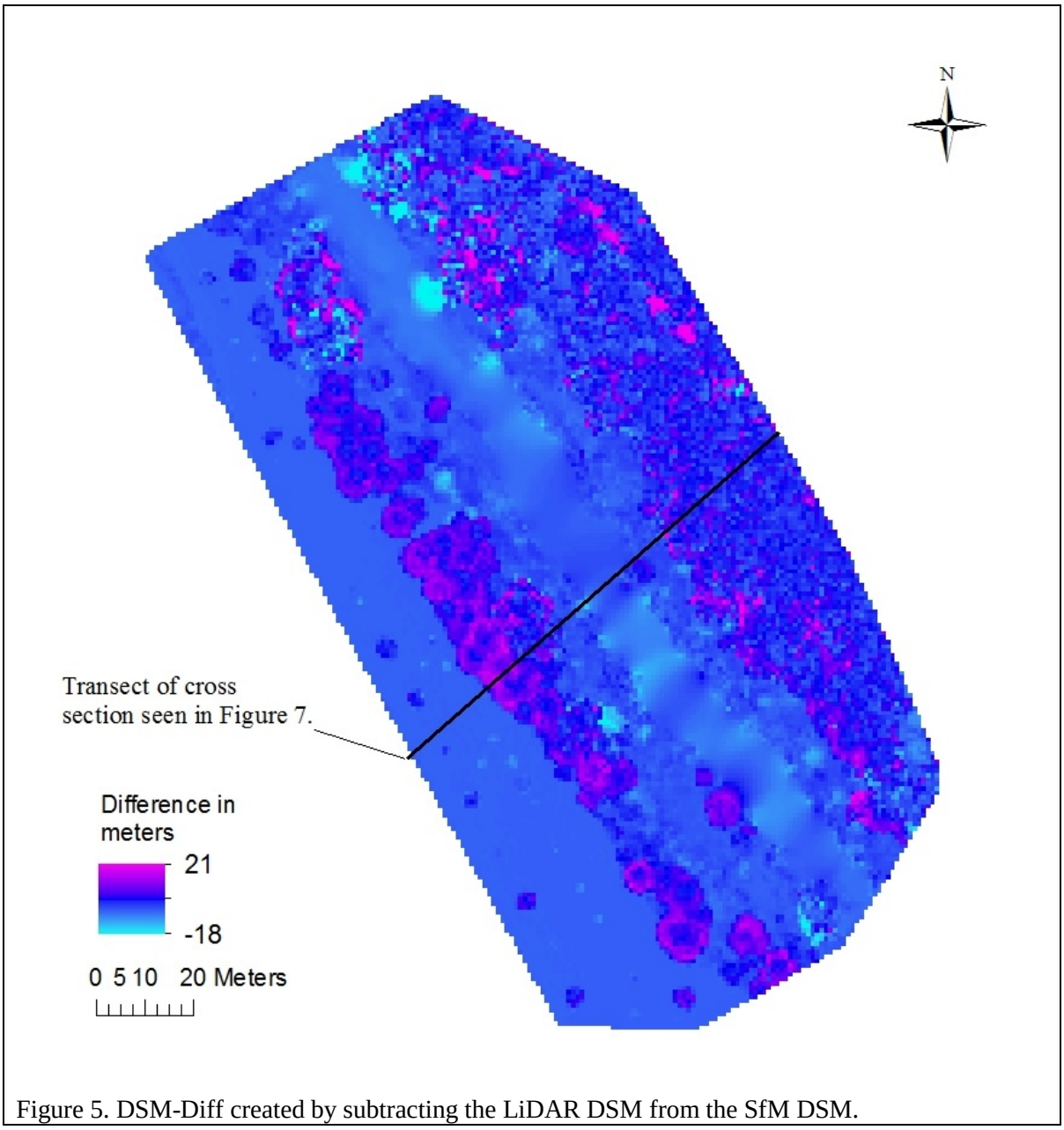

Figure 5. DSM-Diff created by subtracting the LiDAR DSM from the SfM DSM.

Figure 6 presents a cross sectional view of the DSM-Diff where once again the tendency of the elevation values of the SfM DSM to be greater than the elevation values of the LiDAR DSM in forested areas can be seen. In Figure 6 it is possible to see the greater similarity between the SfM DSM and the LiDAR DSM for turf areas than for either deciduous or conifer forest.

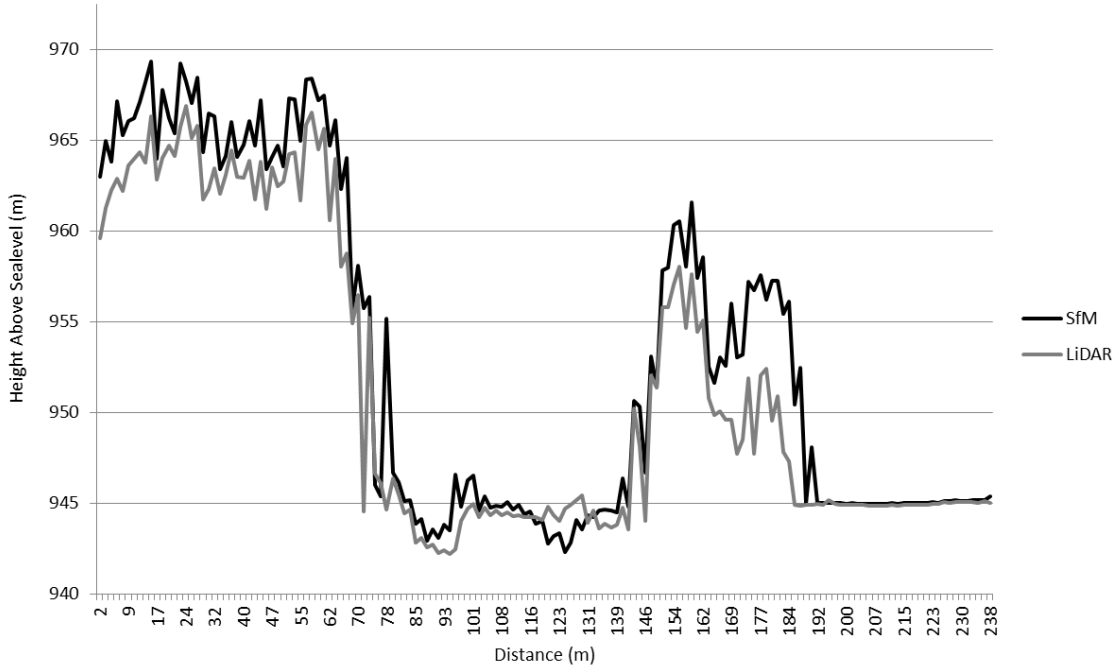

Figure 6. Cross-sectional view comparing the Lidar DSM with the SfM DSM.

Shade model

Using the SfM DSM in conjunction with the GRASS GIS r.sunmask module successfully produced a binary raster file of shade patterns (Figure 7). As can be seen in Figure 7, an initial visual inspection comparing predicted shade to shade as derived from the aerial photographs revealed that modeled shade followed expected patterns; most of the predicted shade shapes closely matched the associated objects casting the shade. That is to say, small round trees appropriately had smaller rounded shade patterns and angular objects, such as the picnic shelters, had square shaped shade patterns.

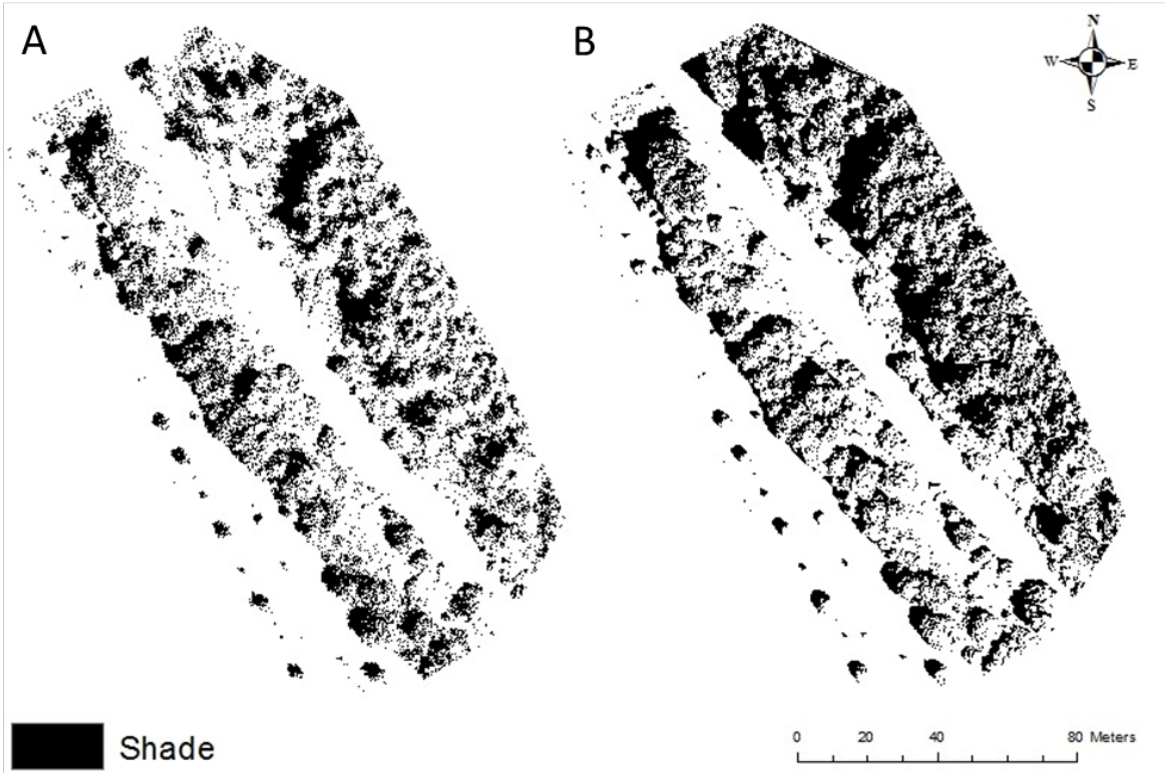

Figure 7. Binary raster layer of reference shade created using the ortho-image (A). Binary raster layer of predicted shade created using the 3-D SfM DSM and GRASS GIS r.sunmask module (B).

A confusion matrix (Congalton, 1991) produced with the two hundred randomly selected check points confirmed that the shade modeling process had resulted in an over prediction of shade in the study area. The overall accuracy of the shade map was 80% with a Kappa Coefficient = 60%. In addition to an overall accuracy the confusion matrix calculated measures for each class known as user's (errors of omission) and producer's (errors of commission) accuracy. User's error refers to the probability that a given point classified as a specific category actually is that category. Producer's error refers to the probability of a given point being correctly assigned to a class. For example, a producer's accuracy = 100% for the shaded category means that 100% of all shaded areas were included in the shade category while a producer's accuracy = 80% for the non-shaded category means that most, but not all non-shaded areas were classified as such. In this example the tendency of the producer is to classify areas as shaded when they are not resulting in the higher producer's accuracy

for the shaded category. For the shade map produced in this study the non-shaded category had a user's accuracy = 98% and a producer's accuracy = 72%. The shade category had a user's accuracy = 62% and a producer's accuracy = 97%.

A confusion matrix produced with the 136 check points randomly selected from flat turf areas and the riverbed found that shade was also over predicted in these areas, but to a lesser extent. Overall accuracy for these locations was 85% with a Kappa Coefficient = 71%. The non-shaded category had a user's accuracy = 100% and a producer's accuracy = 77% while the shade category had a user's accuracy = 70% and a producer's accuracy = 100%.

Analysis of shade shapes for individually selected trees also confirmed that the shade modeling process had over predicted shade (Table 6). In Table 6 it can be seen that for the eleven trees and the one picnic shelter chosen, the area of predicted shade exceeded the area of reference shade by about 14%. Also seen in Table 6 is that predicted shade shapes for trees varied with some having a low percent symmetrical error while for others it was much higher. (These results are discussed in greater detail in the discussion section.) A low percent symmetrical error suggests that two shapes are similar with high overlap while a high percent symmetrical error indicates that two shapes are different or have less overlap. The best was Tree 6, with 25% of predicted shade outside the area of reference shade while the worst was Tree 8 with 176% of predicted shade outside the area of reference shade (Table 6).

Table 6. Predicted Shade Versus Reference Shade for Selected Trees and Picnic Shelter

	Predicted Shade (m^2)	Reference Shade (m^2)	Difference (m^2) (Pred. Shade – Ref Shade)	Percent Symmetrical Error
Tree 1	12.2	12.3	-0.1	31
Tree 2	13.2	11.6	1.6	35
Tree 3	3.2	2.6	0.6	37
Tree 4	19.4	17.9	1.5	25
Tree 5	18.0	15.6	2.4	46
Tree 6	11.0	10.9	0.1	25
Tree 7	4.1	4.1	0	60
Tree 8	8.6	3.8	4.8	176
Tree 9	1.7	1.4	0.3	74
Tree 10	4.1	2.7	1.4	98
Tree 11	6.4	5.8	1.6	100
Picnic Shelter	5.4	4.8	0.6	35
Average	8.9	7.8	1.1	62

Discussion

Point Cloud Characteristics

As previously mentioned, the SfM point cloud produced was extremely dense with a very high number of points (1193 points/m^2 and 3.9 cm spacing). When compared with previous research, this level is on the high end of the scale but within the range of what would be considered typical for 3-D SfM point cloud datasets. For example, Westoby et al. (2012) found point densities of up to 1808 points/m^2 for a 3-D SfM point cloud dataset representing an area of bare earth, exposed rock, and vegetation.

Additionally, greater point densities were found in forested areas than in turf and water areas. This result is consistent with the work of Dandois and Ellis (2013) who similarly found that point cloud densities varied depending on land cover type with forested areas having higher point densities than areas of turf or water. However, Rosnell and Honkavara (2012) found less points were produced in forested areas compared to turf areas. These contrasting results may have occurred due to the use of different software packages. PhotoScan was used for both this study and by Dandois and Ellis (2013) while Bae Systems SOCET SET and Microsoft's Photosynth® were used by Rosnell and Honkavara (2012). How well different land cover types are represented by an SfM point cloud may

be dependent on the proprietary processing methods and algorithms used by different software packages. Thus selecting a software package proven to represent vegetation well may be an important consideration when using SfM methods for ecological modeling applications.

Even with a high level of image overlap and high point density, there were still several locations in forested areas that had no points and left noticeable gaps in the point cloud. All such areas were locations cast in deep shadow by the angle of the sun. Failure of SfM methods to produce points in areas of deep shadow has been noted in previous studies and is a known issue with this technology.

3-D SfM Point Cloud Dataset Accuracies

Accuracy of Turf Areas

The study area encompassed several distinct types of land cover including turf, wetted river bed, and riparian deciduous and evergreen forest. Of these, flat turf areas were the least complex and therefore also the easiest land cover with which to evaluate the quality of the 3-D SfM point cloud dataset. In areas of flat turf the 3-D SfM point cloud dataset appeared to be accurate and of high quality as evidenced by both comparison to the LiDAR DSM and the analysis of 3-D SfM point cloud dataset z value statistics. Analysis of SfM points for the thirty turf plots found the average per plot z value range to be 9.4 cm with a standard deviation of 2.0 cm. Analysis of LiDAR data for the same thirty sample turf areas found the average per plot z value range to be 10.4 cm with a standard deviation of 2.5 cm. Owing to the very flat nature of the turf area, SfM points located there should have been very close together in their z values. The lack of large deviations in z values suggests that little noise existed in the 3-D SfM point cloud dataset. Furthermore, the small range in z values for each sample area validates that these locations were in fact represented as close to flat in the 3-D SfM point cloud dataset. Additionally, the RMSE between the SfM DSM and LiDAR DSM for flat turf areas was low (9.4 cm). As such, the LiDAR point cloud (5 cm vertical RMSE) helped to validate that the 3-D SfM point cloud dataset accurately represented flat turf areas. Such results are consistent with

previous studies that have found high accuracy levels for 3-D SfM point cloud datasets representing flat areas without a high level of vegetative mass. Additionally, a vertical RMSE value of 9.4 cm qualifies for the United States Geological Surveys (USGS) Quality Level 3 Standards for Airborne LiDAR scanning data which require that the vertical RMSE must be less than or equal to 20 cm. Although the vertical RMSE of the SfM DSM was 9.4 cm, the vertical accuracy of the 3-D LiDAR point cloud dataset used as reference was 5.0 cm meaning that the RMSE of the SfM DSM may have been up to 14.4 cm.

Accuracy of Picnic Shelters

In addition to flat turf areas, picnic shelters provided a second convenient place to gauge the accuracy of the 3-D SfM point cloud dataset. Picnic shelters were approximately 270 cm high and easily measured with a measuring tape. As such, they provided distinct objects from which centimeter accuracy reference measurements could be taken. An initial visual inspection of the 3-D SfM point cloud dataset and the SfM DSM found that the picnic shelters were correctly represented as square with straight edges and 90 degree corners and there were no obvious distortions. In addition to the visual inspection, comparing field measurements to measurements taken from the SfM DSM confirmed that the picnic shelters were well represented by the 3-D SfM point cloud dataset. The low vertical and horizontal RMSE (9.6 cm and 9.0 cm respectively) values between picnic shelter heights as measured in the field and picnic shelter heights as measured in the SfM DSM would meet the standards for the USGS Quality Level 2 Airborne LiDAR scanning standards.

Although both picnic shelters had good accuracies, it is interesting to note that each one was represented in the 3-D SfM point cloud dataset with a different degree of accuracy. The most obvious reason for such a difference is that the southern picnic shelter was brightly illuminated by full sun while the north picnic shelter was partially shaded.

Accuracy of Vegetation

Establishing the accuracy with which the 3-D SfM point cloud dataset represented vegetation was more difficult than for either turf areas or picnic shelters. Comparing the LiDAR DSM with the SfM DSM for areas of deciduous and conifer forest resulted in an RMSE = 3.7 and 3.2 m respectively. As a reference, Dandois and Ellis (2013) found an RMSE = 2.3 m when comparing LiDAR and SfM DSMs for an area of deciduous forest. However, in their study the LiDAR data and the SfM data were collected only days apart. One possible reason that the RMSE in this study was not lower is that the LiDAR point cloud was collected in April of 2012 and the SfM imagery was collected late in August of 2014. Vegetation in the study area was at a different stage of seasonal growth and almost three cycles of annual growth had occurred between the LiDAR data collection and the SfM data collection. The difference in foliage present in the study area is illustrated by the fact that in aerial images taken concurrently with the collection of the LiDAR data, four picnic shelters are evident in the study area while in the SfM imagery only two are visible and the remaining two are obscured by tree canopies. Furthermore, the same LiDAR aerial images reveal that a large number of trees in the study area had not yet leafed out, while in the SfM images all trees had full canopies

A better gauge of the accuracy with which vegetation was represented was the comparison between field measured tree heights and the LiDAR/SfM CHM measured tree heights. The high agreement between the two datasets (r^2 = .96, RMSE = 1.25 m) strongly supports that the SfM methods employed in this study were able to accurately represent vegetation height. These results are consistent with studies by Dandois and Ellis (2013) and Lisein et al. (2013) that found field measured tree heights were positively correlated with SfM measured tree heights with values of r^2 = 0.84 and r^2 = 0.91 respectively.

In addition to height, it is also useful to understand how well a point cloud represents the overall shape of vegetation. The results of the shade modeling process provided evidence that vegetation was represented by the 3-D SfM point cloud dataset accurately, but in a simplified form. In

other words, trees were represented as simpler, more compact shapes with definite boundaries instead of complex shapes with amorphous boundaries.

Additionally, the results of the shade modeling process suggest that the accuracy with which the SfM process represented the three dimensional shape of vegetation was affected by the physical characteristics of specific types of trees. There was a better match between predicted shade and reference shade when a tree was geometrically simple with a dense, symmetrical, rounded crown (Figure 8). As can be seen in Figure 8 (D-F), reference shade shape and predicted shade shape were similar for symmetrically simple trees. For such trees the percent error between actual and predicted shade shapes was around 30%, meaning that approximately 70% of predicted shade area was accurate. In Table 7 Trees 1 through 6 are in this geometrically simple category. In contrast, trees with more complex shapes and thinner canopies appeared to be rendered with less accuracy (Figure 8). As can be seem in Figure 8 (A-C), reference shade and predicted shade were quite different for geometrically complex trees. In Table 7 Trees 7 through 11 are in this category. In such cases the SfM process resulted in a truncated shape that often omitted large individual branches extending out from the central area of the tree. This likely occurs due to a difficulty in establishing matching points between photographs for tall thin objects such as single branches (Lisein et al., 2013). For these trees the percent error between actual and predicted shade was on average around 92%. Such a result demonstrates that in these cases shade shape of the predicted shade was very different than the shape of the actual shade.

Figure 8. Apple tree (*Malus Domestics*) where shade was poorly predicted (A) and the same tree with reference shade polygon (B) and predicted shade polygon (C). Example of a Red Maple Trees (*Acer Rubrum*) where shade was predicted more accurately (D) with reference shade polygon (E) and predicted shade polygon (F).

Shade Modeling Process

When an accuracy assessment was used to evaluate shade across the entire study area instead of for individual trees, overall accuracies of 80 percent and 85 percent were found. Although the overall shade accuracies found by this study were reasonable, accuracies of the individual shade and non-shaded categories were respectively lower and higher. Users accuracies for the non-shaded category were very high (user's accuracy = 97% and 100%), while user's accuracies for the shade category were much lower (user's accuracy = 52% and 70%) for both the entire study area and for flat surfaces. In contrast, producer's accuracies for the non-shaded category were lower (producer's accuracy = 72% and 77%), while producer's accuracies for the shade category were much higher (producer's accuracy = 97% and 100%) for both the entire study area and for flat surfaces. The high

producer's accuracy for the shade category is evidence that almost 100% of shaded areas were classified as such. The over prediction of shade ensured that almost all shaded areas were included in the shade category thus resulting in the high shade category producer's accuracy. However, the consequence of the over prediction of shade was that non-shaded areas were also erroneously included in the shade category thus resulting in the lower user's accuracy. In effect, areas identified as non-shaded were rarely shaded but areas identified as shade were often non-shaded and the net result was an over prediction of shade.

As a comparison, Greenberg et al. (2012) used a LiDAR DSM to predict shade cast by vegetation and performed a similar accuracy assessment process. An overall accuracy of 92% was found. Not mentioned was whether or not shade was over or under estimated. One possible reason given for the inaccuracy found was that LiDAR may miss the outermost branches and leaves of vegetation resulting in an under representation of vegetative structure.

For this study it is thought that the shade was over predicted for two reasons. The first is that the SfM DSM is not 3-D in nature but rather what is known as 2.5-D. As such, specific features, such as overhanging branches running parallel to the ground appear in the SfM DSM as a continuous vegetative mass spanning the distance from the ground to the height of the branch (Figure 9). This results in a large over prediction of shade for a given area as sunlight that would pass under the branch and illuminate the ground would be calculated as blocked by the erroneously constructed vegetation. This effect is well illustrated in Figure 9 where actual shade cast by an overhanging branch has a smaller area than predicted shade cast by the 2.5-D model.

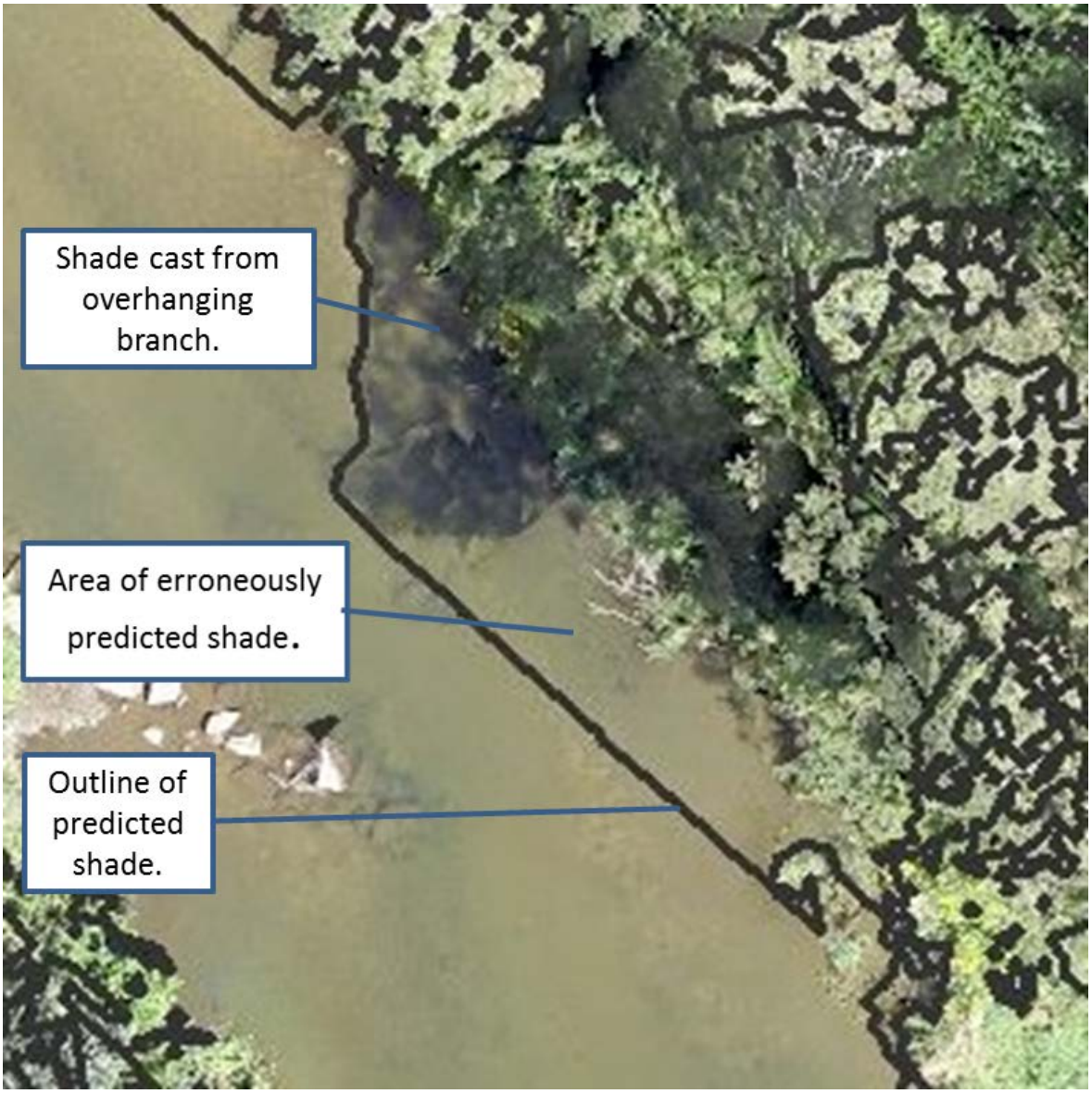

Figure 9. Example of an area where shade was over predicted due to limits of the 2.5-D modeling process.

A second reason for the over prediction of shade is that all surfaces in the SfM DSM are treated as being opaque. In reality, vegetation is a highly complex structure of transparent, semi-transparent and opaque materials. Resultantly, a large amount of the light shining on a tree passes through and creates a pattern that is a mix of sun and shade. In contrast, the completely opaque nature

of the SfM DSM blocks all light, thus creating a homogeneous shade pattern that does not recreate the sun speckled nature of true shadows.

One last factor to be considered when interpreting the results of the shade assessment is that the open nature of the study area created a bias in favor of the non-shaded category. The majority of the non-shaded category was in wide open sections of turf and river with homogeneous solar illumination. In contrast, areas of the shade category were located in or close to vegetation with extremely complex, heterogeneous shade patterns. Resultantly, non-shaded checkpoints were likely to be located in areas where shade was easier to model while shade checkpoints were likely to be located in areas where shade was much harder to model.

The results of the shade accuracy assessment suggest that the applicability of SfM methods for shade modeling is dependent on what surface area the shade is cast upon, and also on the type of vegetation found in the study area. In other words SfM methods may be appropriate for predicting shade cast upon the ground by tree species well represented by SfM methods while being inappropriate for predicting shade cast upon more complex surfaces or by tree species not well represented by SfM methods. For example, the presence of Apple Trees (*Malus Domestics*) with irregular and sparse canopies resulted in a gross over prediction of shade while Red Maple Trees (*Acer Rubrum*) with full, rounded canopies resulted in a more accurate shade prediction. Additionally, predicted shade was more accurate for flat areas such as turf and water (Overall accuracy = 85%) than for the study area as a whole (Overall accuracy = 80%). This is likely due to the fact that much of the study area was covered by forest canopy with its extremely complex and heterogeneous shade patterns. Predicting shade across the vegetative canopy was extremely challenging as the surface is highly irregular and semi-transparent to sunlight. In contrast, modeling shade in flat turf areas and the river was simpler.

Conclusion

A UAS system was successfully designed and utilized to collect a set of photographs appropriate for the purpose of constructing a 3-D point cloud dataset using SfM methods. From those photographs a 3-D point cloud was created that represented all land cover types (turf, river, deciduous and conifer forest) in the study area with an adequate density of points. Comparison of a DSM derived from the 3-D SfM point cloud dataset with a LiDAR derived DSM resulted in a good fit for turf areas and a moderate fit for areas of deciduous and conifer forest. The fit for turf areas was good enough to qualify for the United States Geological Surveys (USGS) Quality Level 3 Standards for Airborne LiDAR scanning data which require that the vertical RMSE must be less than or equal to 20 cm. A high level of both vertical and horizontal accuracy was found when ground truth building heights and widths were compared with building heights and widths derived from the 3-D SfM point cloud dataset. Tree heights established from a LiDAR/SfM CHM were highly predictive ($r^2 = 0.96$) of tree heights established through ground truth methods. The use of the GRASS GIS module r.sunmask to predict shade patterns using a DSM derived from the 3-D SfM point cloud data set found that horizontal and vertical accuracies of vegetation as represented by the DSM appeared to be dependent on the characteristics of vegetation with compact, round trees being represented more accurately than trees with complex shapes.

Overall, the results of this study support that SfM methods are affordable, highly mobile, and can be used for scientific studies of vegetation depending on the level of accuracy required and the type of vegetation involved. Although the results produced by this study were less accurate than those produced by professional ALS methods, they were also much less expensive with a one-time cost of only approximately $13,000 required. Additionally, the methods employed were highly mobile and able to be deployed on short notice at the discrepancy of the researcher using the data. This opens up the possibilities for capturing 3-D data at a high temporal resolution.

One possible application of the SfM methods employed by this study is the documentation of changes to vegetation occurring at or above the meter level. For example, changes resulting from

human caused events, such as logging, or stochastic events such as forest fires or die-offs of trees from disease could be documented using SfM methods. Such events result in changes to canopy height on the order of several meters and could thus be documented using SfM methods with an error bound such as was found in this study. Another potential application of SfM methods is studies researching the effects of solar irradiation on riverine ecosystems. Despite the limitations of the methods employed, an overall accuracy level of 85% was found for shade predictions in the area of the river. Depending on the specific nature of the study, such an accuracy level may be acceptable.

.

References

Agisoft, 2014. Agisoft PhotoScan user manual, professional edition, version 1.1., URL: http://www.agisoft.com/pdf/photoscan-pro_1_1_en.pdf (last date accessed: March 19, 2015).

Bryson, M., M. Johnson-Roberson, R. J. Murphy, and D. Bongiorno, 2013. Kite aerial photography for low-cost, ultra-high spatial resolution multi-spectral mapping of intertidal landscapes, *Plos One* 8 (9): e73550.

Canon U.S.A, 2014. Canon PowerShot S100 brochure, URL: http://www.usa.canon.com/cusa/ support /consumer/digital_cameras/powershot_s_series/ powershot_s100 (last date accessed: March 19, 2015).

Colby, J. D., and J. G. Dobson, 2010. Flood modeling in the coastal plains and mountains: analysis of terrain resolution, *Natural Hazards Review* 11 (1): 19–28.

Colomina, I., and P. Molina, 2014. Unmanned aerial systems for photogrammetry and remote sensing: a review, *ISPRS Journal of Photogrammetry and Remote Sensing*, 92 (June): 79–97.

Congalton, R. G., 1991. A review of assessing the accuracy of classifications of remotely sensed data, *Remote Sensing of Environment*, 37: 35-46.

Dandois, J. P., and E. C. Ellis, 2013. High spatial resolution three-dimensional mapping of vegetation spectral dynamics using computer vision, *Remote Sensing of Environment*, 136 : 259–76.

Dey, D., L. Mummert, and R. Sukthankar, 2012. Classification of plant structures from uncalibrated image sequences, *Applications of Computer Vision (WACV), 2012 IEEE Workshop on:*, 9-11 Jan 2012, Breckenridge, CO, pp . 329 – 336.

DJI, 2014. DJI Phantom 2 Vision + Brochure, URL: http://www.dji.com/product/phantom-2-vision-plus (last date accessed: March 19, 2015).

Erdody T., and L.M. Moskal, 2010. Fusion of lidar and imagery for estimating forest canopy fuels, *Remote Sensing of Environment*, 114(4); 725-737.

Fonstad, M. A., J. T. Dietrich, B. C. Courville, J. L. Jensen, and P. E. Carbonneau, 2013. Topographic structure from motion: a new development in photogrammetric measurement, *Earth Surface Processes and Landforms* 38 (4): 421–30.

Geodetic Systems, 2014. What is photogrammetry website, URL: http://www.geodetic.com/v-stars/what-is-photogrammetry.aspx (last date accessed: April 21, 2015).

Greenberg, J. J., E. L. Hestir, D. Riano, G. J. Scheer, and S. L. Ustin, 2012. Using LIDAR data analysis to estimate changes in insolation under large-scale riparian deforestation, *Journal of the American Water Resources Association* 48, no. 5 (October): 939-947.

Goode, P. J., 1927. Presidential Address: The map as a record of progress in geography, *Annals of the Association of American Geographers*, 17(1).

GoPro, 2014. GoPro Hero4 Black Edition brochure, URL: http://shop.gopro.com/hero4/hero4-black/CHDHX-401.html (last date accessed: March 19, 2015).

Guedet, P., G. Wells, D. Maidment, and A. Neuenschwander, 2004. Influence of the post spacing of the LiDAR-derived DEM on flood modeling, *Proceedings of the 2004 American Water Resources Association Spring Specialty Conf., GIS and Water Resources III, AWRA*, 30 May 2004, Nashville, Tenn.

Harwin, S., and A. Lucieer, 2012. Assessing the accuracy of georeferenced point clouds produced via multi-view stereopsis from unmanned aerial vehicle (UAV) imagery, *Remote Sensing* 4 (6): 1573–99.

Heidemann, H. K., 2014. LiDAR base specification, Chapter 4 of Section B, U.S. Geological Survey Standards, Book 11, Collection and Deliniation of Spatial Data. URL: http://pubs.usgs.gov/tm /11b4/pdf/tm11-B4.pdf (Date last accessed: March 24, 2015).

Hodgson, M. E., and P. Bresnahan, 2004. Accuracy of airborne lidar-derived elevation: empirical assessment and error budget, *Photogrammetric Engineering and Remote Sensing* 70 (3): 331–39.

Hummel, S., A. T. Hudak, E. H. Uebler, M. J. Falkowski, and K. A. Megown, 2011. A comparison of accuracy and cost of lidar versus stand exam data for landscape management on the Malheur National Forest, *Journal of Forestry* 109 (5): 267–73.

Lefsky, M.A., W.B. Cohen, G.C. Parker, and D.J. Harding, 2002. LiDAR remote sensing for ecosystem studies, *Bioscience* 52(1): 19-30.

Lisein, J., M. Pierrot-Deseilligny, S. Bonnet, and P. Lejeune, 2013. A photogrammetric workflow for the creation of a forest canopy height model from small unmanned aerial system imagery, *Forests* 4 (4): 922–44.

Lucieer, A., S. M. de Jong, and D. Turner, 2014. Mapping landslide displacements using structure from motion (SfM) and image correlation of multi-temporal UAV photography, *Progress in Physical Geography* 38 (1): 97–116.

Mathews, A.J., and J. L. R. Jensen, 2013. Visualizing and quantifying vineyard canopy LAI using an unmanned aerial vehicle (UAV) collected high density structure from motion point cloud, *Remote Sensing* 5 (5): 2164–83.

Newcomb, D., 2012. Using GRASS GIS to model solar irradiation on North Carolina aquatic habitats with canopy data. *Transactions in GIS* 16(2): 161-176.

Rosnell, T., and E. Honkavara, 2012. Point cloud generation from aerial image data acquired by a quadrocopter type micro unmanned aerial vehicle and a digital still camera, *Sensors* 12 (1): 453–80.

SenseFly, 2014. senseFly eBee Brochure, URL: https://www.sensefly.com/drones/ebee.html (date last accessed: March 20, 2015).

Snavely, N., S. M. Seitz, and R. Szeliski, 2006. Photo tourism: exploring photo collections in 3-D, *Acm Transactions on Graphics* 25 (3): 835–46.

Tobler, W. R., 1988. Resolution, resampling and all that, *Building Databases for Global Science: Proc,. 1st Meeting of the Int. Geographical Union Global Database Planning Project*, H. Mounsey and R. F. Tomlinson, eds., Taylor and Francis, London, 129-137 p.

Trimble Navigation Limited, 2014. Trimble GNSS survey systems brochure, URL: http://trl.trimble.com/ docushare/dsweb/Get/Document-270097/022543-366F_GNSS_Portfolio_BRO_1014_LR.pdf (last date accessed: March 19, 2015).

Turner, A. B., J. D. Colby, R. M. Csontos, and M. Batten, 2013. Flood modeling using a synthesis of multi-platform LiDAR data, *Water*, *5*(4), 1533-1560.

Verhoeven, G., 2011. Taking computer vision aloft - archaeological three-dimensional reconstructions from aerial photographs with PhotoScan, *Archaeological Prospection* 18 (1): 67–73.

Westoby, M. J., J. Brasington, N. F. Glasser, M. J. Hambrey, and J. M. Reynolds, 2012. Structure-from-motion' photogrammetry: a low-cost, effective tool for geoscience applications, *Geomorphology* 179 (December): 300–314.

Biographical Sketch

James Balcomb received his Master of Arts from the Appalachian State University Department of Geography and Planning in May 2015. James received his B.S. in Natural Resources Planning and Interpretation from Humboldt State University of Arcata, California. After graduating from Humboldt State University James worked seasonal jobs as a wildland firefighter, backcountry ranger and assistant park manager. In 2005 James went to work for the alternative energy industry in Boulder Colorado where he spent seven years installing photovoltaic power systems on residential structures.

James' academic interests include the use of geographical information systems (GIS) and remote sensing for deriving solutions to environmental issues. In particular, James is interested in the use of three dimensional modeling techniques, such as LiDAR and computer vision to collect the data needed for creating and running ecological modeling.